Nitrogen Reduction by Multimetallic Trans-Uranium Actinide Complexes: A Theoretical Comparison of Np and Pu to U

Dipak Panthi, Olajumoke Adeyiga, Naveen K. Dandu and Samuel O. Odoh*

Department of Chemistry, University of Nevada Reno, 1664 N. Virginia Street, Reno, NV 89557-0216

Email Addresses:

dpanthi@unr.edu

oadeyiga@unr.edu

ndandu@unr.edu

sodoh@unr.edu

ABSTRACT: There is recent interest in organometallic complexes of the trans-uranium elements. However, preparation and characterization of such complexes are hampered by radioactivity and chemo-toxicity issues as well as the air-sensitive and poorly understood behavior of existing compounds. As such, there are no examples of small molecule activation via redox reactivity of organometallic trans-uranium complexes. This contrasts with the situation for uranium. Indeed, a multimetallic uranium (III) nitride complex was recently synthesized, characterized and shown to be able to capture and functionalize molecular nitrogen (N_2) through a four-electron reduction process, $N_2 \rightarrow N_2^{4-}$. The bis-uranium nitride, U-N-U core of this complex is held in a potassium siloxide framework. Importantly, the N_2^{4-} product could be further functionalized to yield ammonia (NH_3) and other desirable species. Using the U-N-U potassium siloxide complex, K_3U-N-U, and its cesium analogue, Cs_3U-N-U, as starting points, we use scalar-relativistic and spin-orbit coupled density functional theory (DFT) calculations to shed light into the energetics and mechanism for N_2 capture and functionalization. The $N_2 \rightarrow N_2^{4-}$ reactivity depends on the redox potentials of the U(III) centers and crucially on the stability of the starting complex with respect to decomposition into the mixed oxidation U(IV)/U(III) K_2U-N-U or Cs_2U-N-U species. For the trans-uranium, Np and Pu analogues of K_3U-N-U, the $N_2 \rightarrow N_2^{4-}$ process is endoergic and would not occur. Interestingly, modification of the Np-O and Pu-O bonds between the actinide cores and the coordinated siloxide framework to Np-NH, Pu-NH, Np-CH_2 and Pu-CH_2 bonds drastically improves the reaction free energies. The Np-NH species are stable and can reductively capture and reduce N_2 to N_2^{4-}. This is supported by analysis of the spin densities, molecular structure, long-range dispersion effects as well as spin-orbit coupling effects. These findings chart a path for achieving small-molecule activation with organometallic neptunium analogues of existing uranium complexes.

1. INTRODUCTION

Nitrogen in chemically accessible forms is very important in agriculture and the chemical industry. Nitrogen is abundant in the atmosphere as dinitrogen, N_2. N_2 is however very stable and chemically unreactive because of its high binding energy, high ionization potential and negative electron affinity.[1,2] Nitrogenase enzymes in some microbes can activate and reduce N_2 to accessible forms under ambient conditions. The biological fixation of N_2 to ammonia, NH_3, is however not sufficient to support the ever-growing global population. As such, there has long been interest in understanding the detailed mechanism of the biological N_2 fixation process and in the development of synthetic, industrially viable and catalytic approaches for converting N_2 to NH_3.[1-8] The Haber-Bosch process is an industrial approach for achieving this conversion.[9] This process employs a heterogenous iron catalyst, albeit under very harsh conditions of high temperatures and pressures. The requirements of the Haber-Bosch process are so high that it consumes about 1% of the global energy supply.[10] Early attempts at developing well-characterized transition metal complexes that can reduce nitrogen under ambient conditions focused on Mo and W species, culminating in various discoveries.[3,6,11-16] There have also been many reports describing the activation and subsequent one-, two- and three-electron reduction of N_2 by lanthanide complexes.[17-25] In many cases the binding of N_2 by lanthanide complexes is coupled to a II/III oxidation state redox couple of the 4*f* metal site and an external electron source. Interestingly, many of the lanthanide species that have been reported are multimetallic species, containing 2-4 lanthanide atoms.[22,23,25] Due to these developments, it is now recognized that many transition metal and lanthanide complexes can bind and reduce N_2.[6,8,10,11,19] However, transformation of the reduced species to intermediates containing N-H and N-C bonds remains a significant challenge.[26]

Prior to the development and commercialization of the Haber-Bosch process, it was known that uranium and uranium nitride were most effective for producing NH_3 from N_2.[26,27] There are however few uranium complexes in the +3 oxidation state, U(III), capable of binding and reducing N_2. Recently, Falcone et al. reported a multimetallic U(III) nitride complex, Figure 1, able to bind and direct the 4-electron reduction of N_2 ($N_2 \rightarrow N_2^{4-}$).[26] The active site in this complex is a bis-uranium nitride core, U-N-U, encased within a potassium siloxide framework. The potassium siloxide framework provides an ideal conformation and sufficient flexibility to accommodate the binding and reduction of N_2. In the 4-electron reduction process, the two U(III) centers are oxidized to the +5 oxidation state, forming an intermediate U(V)/U(V) U-(N)(N_2)-U complex, Figure 1. Falcone et al. discovered that addition of protons to U-(N)(N_2)-U generates stoichiometric amounts of NH_3. Likewise, addition of CO led to the formation of N-C bonds, providing

a route to the development of organonitrogen species.[26] This report is in line with several others showing the utility of U(III) for small molecule activation.[26,28-36]

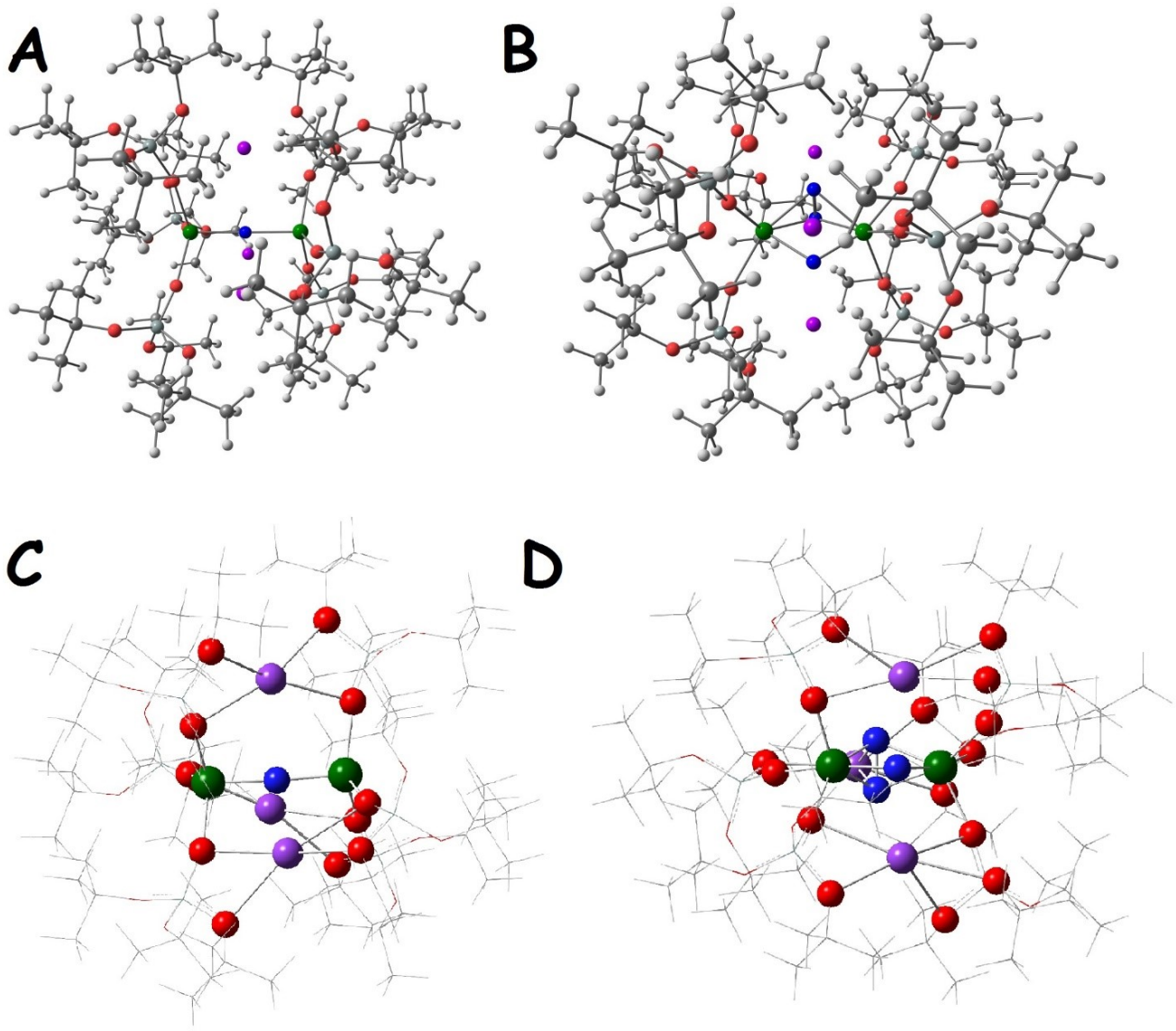

Figure 1: Structure of the (A) U-N-U core and (B) U-N(N_2)-U cores encased in the potassium siloxide framework. We use wireframes to allow for better visibility of the actinide nitride cores of these complexes in (C) and (D), respectively. In all cases, the H, C, N, O, P and U are atoms are depicted with white, grey, blue, red, purple and green spheres, respectively.

Our interests lie in exploring the differences between uranium chemistry and the chemistry of the trans-uranium elements. To illustrate, there is no report on the ability of trivalent neptunium, Np(III), complexes to effect redox reactivity for small molecule activation. A possible reason is the paucity of suitable radiological laboratories for trans-uranic chemical investigations.[37] Beyond uranium, the

elements become more chemotoxic and in many cases, more radioactive. Thus, experimental setups for trans-uranium chemistry are more complicated, often requiring significant radioprotection to avoid exposure to radioactive materials. There is however some progress in the development of laboratories and instrumentation suitable for the synthesis and characterization of trans-uranic species. It will therefore possible that Np(III) complexes that are useful for small molecule activation will be developed in the future. Insights from experimental and theoretical investigations will facilitate the development of ligand frameworks able to drive changes in the formal oxidation states of Np during small molecule activation. Theoretical quantum mechanical calculations can be used to compare the electronic structure and chemical properties of U(III) systems to those of their Np(III) analogues in order to shed light on any differences between small molecule activation by these species. These calculations could also provide insights into ligand modifications useful for altering the redox reactivity of the Np complexes. This is important as organometallic Np complexes are relatively rare.

In this work, we have used quantum mechanical computations to examine the structural, electronic and chemical properties of the bimetallic U-N-U complex implicated in N_2 binding and reduction by Falcone et al.[26] We compare the properties of this U(III) system to those of its Np and Pu analogues, Scheme 1. The Pu species have been included to allow for detailed comparison of the trends in the behaviors of the early actinides. We focus on the energetics associated with the binding and reduction of N_2 as given in Scheme 1. By comparing the redox reactivity for U(III) to those of Np(III) and Pu(III), we aim to unravel differences in the properties of these actinide species. We also examine the effects of modifying the ligand environment around the actinide centers by replacing the coordinated oxo groups of the siloxide framework with NH and CH_2 moieties. We examine whether alteration of the ligands can drive redox small-molecule reactivity in the Np(III) and Pu(III) systems.

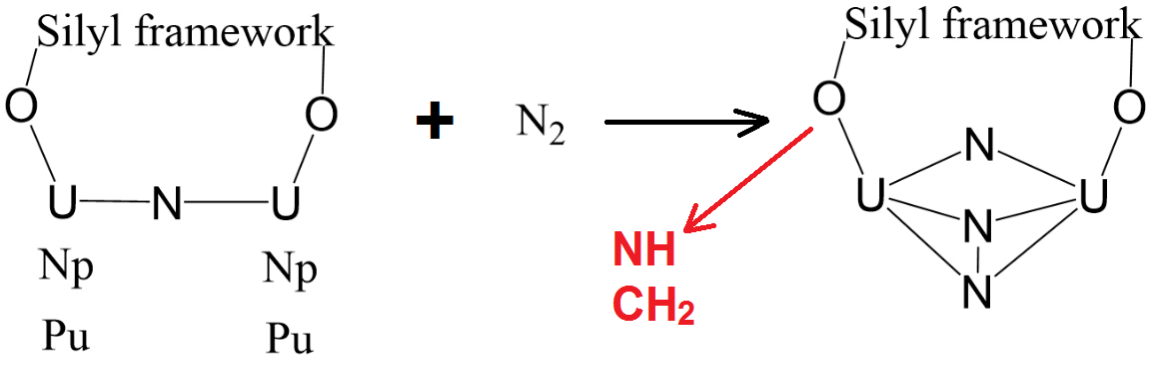

Scheme 1: Binding and reduction of N_2 by the U-N-U core encased in a potassium siloxide (oxo-silyl) core. We are interested in the reactivity of analogous Np and Pu complexes as well as situations where the oxo groups bound to the actinide centers are replaced by NH or CH_2 groups.

2. COMPUTATIONAL DETAILS

Geometry optimizations and vibrational frequency analyses were carried out in the gas phase with all-electron (AE) basis sets at the scalar relativistic level while employing the Priroda code.[38-40] The experiments of Falcone et al. were performed by exposing the crystalline materials directly to N_2 gas.[26] We used the Perdew-Burke-Ernzerhof (PBE) generalized gradient approximation (GGA) density functional in these calculations.[41] GGA functionals can mimic the effects of static electron correlation energy although in an unspecified manner.[42] The PBE functional is within 3-4 kcal/mol of complete active space second-order perturbation theory (CASPT2) and coupled-cluster theory, CCSD(T) and CCSDT, when used to compute the energies associated with redox reactions involving several actinide species, Tables S3, S4 and S5 of the Supporting Information.

We used AE basis sets labelled here as L1 and of double-ζ-polarized quality for the large component and corresponding kinetically balanced basis sets for the small components. Specifically, the actinide atoms were described with 34s33p24d18f6g contracted to 10s9p7d4f1g while the second-row elements were described with 10s7p3d contracted to 3s2p1d. The silicon and hydrogen atoms were described with 15s11p3d (contracted to 4s3p1d) and 6s2p (contracted to 2s1p), respectively.[38] The scalar-relativistic approach that we have employed is based on the full Dirac equation but with spin-orbit terms projected out and neglected. The details of this approach have been previously described.[43] The positions of all the atoms were relaxed during the geometry optimizations and no symmetry constraints were imposed. In order to provide insights into the N_2 reduction process, the electronic structures of the actinide complexes were analyzed with Mayer bond orders,[44] Mulliken atomic charges and spins[45] and inspection of the frontier orbitals. Tests on truncated versions of the complexes show that the Mulliken spins calculated at the PBE/L1 level are close to the Hirshfeld charges[46] and yield similar number of electrons associated with the $N_2 \rightarrow N_2^{4-}$ transformation, see Table S2 of Supporting Information. The change in electronic energies, ΔE, and free energies, ΔG, associated with the $N_2 \rightarrow N_2^{4-}$ process, Scheme 1, are described with **I** and **II** respectively. On the reactant side (An-N-An), we consider the N_2 molecule and the actinide complex as being infinitely separated. The actinide atoms are depicted as "An" while the products, Scheme 1, are depicted as An-(N)(N_2)-An in **I** and **II**.

$$\Delta E_{scalar} = E_{\mathrm{An-(N)(N_2)-An}} - E_{\mathrm{An-N-An}} - E_{\mathrm{N_2}} \qquad \textbf{(I)}$$

$$\Delta G_{scalar} = G_{\mathrm{An-(N)(N_2)-An}} - G_{\mathrm{An-N-An}} - G_{\mathrm{N_2}} \qquad \textbf{(II)}$$

The contributions of dispersion effects to the reaction energy were estimated with the DFT-D3 scheme of Grimme et al.[47,48] while using the Becke-Johnson damping scheme to avoid divergence of dispersion

energy at small inter-atomic distances[49], DFT-D3(BJ). These corrections to ΔG_{scalar} were incorporated according to **III**. We used the DFT-D3 calculator implemented in the Gaussian 16 code[50] with PBE, PBE-D3BJ. The optimized geometries from Priroda were used in these calculations.

$$\Delta G_{scalar-disp} = \Delta G_{scalar} + \Delta E_{dispersion\ energy} \qquad \textbf{(III)}$$

In all these calculations, we considered only the low- and high-spin states for the complexes. In general, these states correspond to the broken-symmetry singlet and ferromagnetic arrangement of the 5*f* electrons. The broken-symmetry singlet state corresponds to an open-shell singlet state with the spin of a local site flipped from the high-spin state to allow for antiferromagnetic coupling of the actinide centers. A quick check showed that intermediate spin states are higher in energy. The high-spin states of the U(III)/U(III), Np(III)/Np(III) and Pu(III)/Pu(III) complexes are septet, nonet and undecet, respectively, while those of the oxidized U(V)/U(V), Np(V)/Np(V) and Pu(V)/Pu(V) species are triplet, quintet and septet, respectively.

To estimate the effects of spin-orbit coupling on the reaction energies, we have chosen to truncate the bulky actinide complexes to the central bis-actinide nitride, An-N-An (where An = U, Np and Pu) and An-(N)(N_2)-An cores, Scheme 1. To imitate the charge distributions in the bulky complexes, we have included the immediate ligand atom(s) coordinated to the actinide sites (O, NH or CH_2) and then balanced the charges by adding protons. The positions of the capping protons were optimized at the B3LYP-D3BJ/def2-TZVPP level[47-49,51-53] while keeping all other atoms in positions obtained from optimization of the full molecules in Priroda.[38-40] The actinide centers were described with Stuttgart small-core effective core potentials and associated valence basis sets. We used two approaches to include spin-orbit coupling effects within the scope of DFT. In the first, we used the NWChem[54] suite of programs while describing all atoms with CRENBL (Christiansen, Ross, Ermler, Nash, Bursten, and Large-valence-shape-consistent) relativistic effective core potentials (ECP).[55-58] We performed calculations with and without spin-orbit operators on all atoms.[55] The DFT and spin-orbit DFT, SODFT, calculations were carried out with the B3LYP density functional.[59] The SODFT approach is expected to be moderately accurate for the reaction energies.[59-61] It is computationally efficient and was used for all the $N_2 \rightarrow N_2^{4-}$ processes that we examined. The spin-orbit coupling effects were used to correct **III** thus:

$$\Delta G_{spin-orbit} = \Delta G_{scalar-disp} + \Delta E_{spin-orbit\ with\ B3LYP} - \Delta E_{scalar-relativistic\ with\ B3LYP} \qquad \textbf{(IV)}$$

In the second approach, we carried out scalar-relativistic and spin-orbit calculations with the ADF code[62-64] while utilizing the zero-order regular approximation (ZORA)[65] and slater-type triple-ζ double-polarized (TZ2P) orbitals on all atoms.[66-68] These calculations were performed on the U complexes only

and were used to estimate the reliability of the ECP approach. The 1*s*-4*f* orbitals of the U atoms as well as 1*s* orbitals of the N and O atoms were regarded as core orbitals and were kept frozen. We used the PBE functional for these calculations.

3. RESULTS AND DISCUSSION

3.1. Structural and Electronic Properties of the U(III) and U(V) Complexes: In Table 1, we compare the X-ray crystallographic and DFT-optimized structural parameters of the broken symmetry and high-spin states of the U-N-U and U-(N)(N_2)-U potassium siloxide complexes. For the U-N-U potassium

Table 1: Average values of the calculated structural parameters of the bis-actinide U-N-U and U-(N)(N_2)-U complexes with a potassium siloxide framework are compared to available experimental data.[26] The bond distances are given in Å while the bond angles are given in °.The average bond orders for selected bonds are given in parenthesis. We used average values as the molecules are not completely symmetric.

	K_3U-N-U			K_3U-(N)(N_2)-U		
	Singlet	Septet	Expt.	Singlet	Triplet	Expt.
U-N_{center}	2.107 (1.61)	2.115 (1.61)	2.120	2.109 (1.59)	2.112 (1.46)	2.071
U-$N_{dinitrogen}$				2.215 (1.06)	2.213 (1.04)	2.163-2.311
U-U	4.199	4.223	4.234	3.346 (0.71)	3.341 (0.73)	3.305
U-O	2.261 (0.74)	2.261 (0.74)	2.288	2.271 (0.75)	2.271 (0.74)	2.229
K-O	2.867	2.872	2.819	2.658-3.642	2.611-3.812	2.535-3.282
N-$N_{dinitrogen}$				1.490 (0.96)	1.493 (0.93)	1.521
U-N_{center}-U	170.5	174.5	173.7	105.0	104.6	105.9
U-$N_{dinitrogen}$-U				97.9 & 98.3	97.8 & 98.2	93.3-97.8

siloxide complex, K_3U-N-U, the high-spin septet state provides structural parameters in better agreement with the experimental data than the broken-symmetry singlet state.[26] This is interesting as we found the singlet and septet states to be nearly iso-energetic, based on the calculated electronic energies. The energy difference between these states is about 1.2 kcal/mol at the PBE level. With dispersion effects, the energy difference is around 1 kcal/mol. For the bonds around the U-N-U core, the optimized structure of the septet state are within 0.02 Å (for bond lengths) and 0.8°(for the U-N-U bond angle) of the experiment.[26] The distances between the oxygen atoms of the siloxide framework and the potassium centers are over-estimated by DFT, by about 0.05 Å. This is likely because our geometry optimizations did not account for long-range dispersion effects. However, an error of 0.05 Å corresponds to only about 1.8 % of the

experimental bond lengths.[26] The accuracy of the geometrical parameters obtained for the K_3U-N-U complex gives us confidence regarding our theoretical model. The central nitride atom of K_3U-N-U is labeled as N_{center} in Table 1.

Similar to the case for K_3U-N-U, the bond lengths near the bis-uranium core of K_3U-(N)(N_2)-U are within 0.05 Å of the experimental data while the bond angles are within 1-5° of the experiment. Comparison of the optimized and experimental structures of the K_3U-N-U and K_3U-(N)(N_2)-U complexes indicate that binding of N_2 is associated with significant opening of the siloxide framework, Figure 1.[26] It seems crucial that the framework is sufficiently flexible to accommodate the collapse of the U-N_{center}-U bond angle from about 173° to around 106°, Table 1. The average K-O distances also become significantly elongated after N_2 capture. This is adequately reproduced in our optimized geometries. The atoms of the captured N_2 moiety of K_3U-(N)(N_2)-U are labeled as $N_{dinitrogen}$ in Table 1.

At the PBE/L1 scalar-relativistic level, the Mayer bond order[44] of gaseous N_2 is 3.02. This is indicative of a triple bond. In K_3U-(N)(N_2)-U, the bond order between the atoms of the bound N_2 moiety is 0.96 (single bond), illustrating the loss of two bonds, Table 1. There are however now four bonds between the U centers and the atoms of the captured N_2, Scheme 1. These U-N bonds have bond orders of about 1.06. It therefore appears that N_2 capture is associated with lysis of two bonds in N_2 and the simultaneous formation of four U-N bonds. This is indicative of the transfer of four electrons from the U atoms to N_2, a fact confirmed by examining the spin densities of the U atoms. For the broken-symmetry singlet states, the U spin densities are 3.25 and -3.24 for K_3U-N-U, confirming their $5f^3$ or U(III) characters. In contrast, the U spin densities are -1.20 and 1.21 in K_3U-(N)(N_2)-U, confirming their $5f^1$ or U(V) character. For the high-spin states, K_3U-N-U has spin densities of 3.06 and 3.00 on the U centers while they are reduced to 1.17 and 1.18 in K_3U-(N)(N_2)-U. Interestingly, the collapse of the U-N_{center}-U bond angle during the $N_2 \rightarrow N_2^{4-}$ process is associated with the formation of a *near*-single-bond between the U(V) centers of K_3U-(N)(N_2)-U. A bond order of 0.71 is associated with the U-U distance of this complex, Table 1.

One of the factors that determine whether K_3U-N-U can bind and reduce N_2 is the redox potentials of the U(III) sites. This can be studied in a qualitative manner by comparing the eigenvalues of the frontier orbitals of this complex to those of gaseous N_2. In Figure 2, we show that the π* orbitals of unbound N_2 are 1.58 eV below the vacuum level. Interestingly, we find that four out of the six U 5*f* electrons of K_3U-N-U are -1.42 to -1.46 eV below the vacuum level in the ground singlet state (and -1.38 to -1.44 eV for the septet state). As such, there is no '*barrier*' to the transfer of these four electrons to the π* orbitals of N_2, in so far as N_2 can approach the U-N-U core. As the U-N-U moiety is embedded deeply in the siloxide

framework, Figure 1A, it is reasonable to expect that capture and reduction of N_2 will be associated with opening of the framework. Thus, framework flexibility is crucial. That said, it is also important that the interactions between the U-N-U core and the siloxide framework is strong. Situations with relatively weak interactions between the U-N-U core and the siloxide framework could result in complicated reactivity associated with formation of decomposition products.[69]

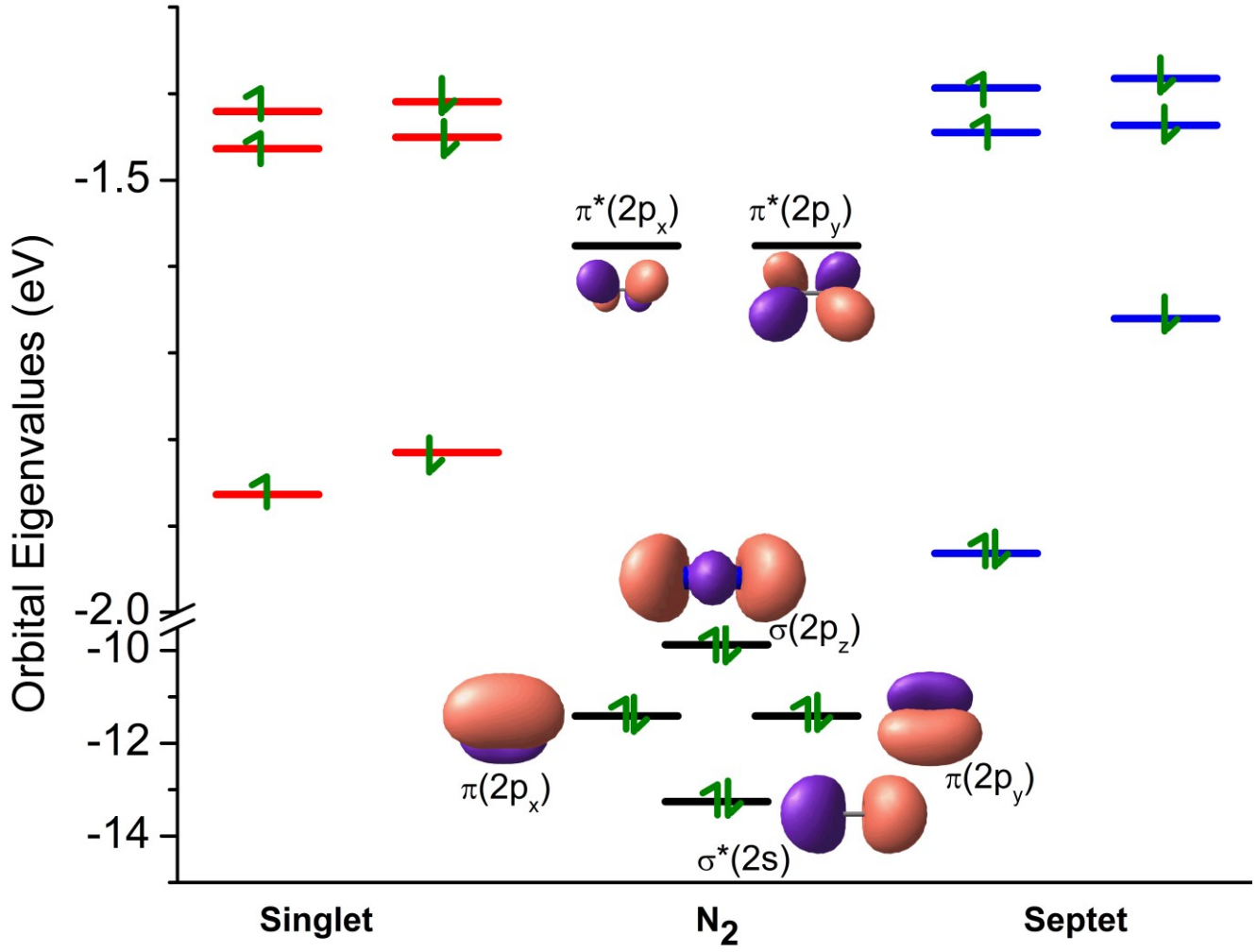

Figure 2: Comparison of the eigenvalues of the frontier orbitals of N_2 to those of the broken-symmetry singlet (red) and septet (blue) states of the U-N-U potassium siloxide complex. The eigenvalues were obtained at the PBE/L1 scalar-relativistic level.

3.2. Energetics of N_2 Reduction by U(III) Species: Experimentally, Falcone et al. found that while K_3U-N-U efficiently reduces N_2,[26] its cesium analogue, Cs_3U-N-U, leads to less-defined reactivity due to the formation of decomposition products.[69] The calculated reaction energies for $N_2 \rightarrow N_2^{4-}$ conversion by K_3U-N-U is presented in Table 2. The electronic reaction energy is -51.9 kcal/mol at the PBE/L1

level. Thermal Gibbs free energy corrections reduce the reaction energy by 20.2 kcal/mol while corrections for long-range dispersion interactions favor reactivity by 10.5 kcal/mol while spin-orbit coupling favors endoergicity by 1.0 kcal/mol respectively. The energy contributions due to spin-orbit coupling effects were obtained with the CRENBL spin operators approach. With all-electron basis sets and the ZORA Hamiltonian, the magnitude of the contributions from spin-orbit coupling remain relatively unchanged, 4.7 kcal/mol, also favoring endoergicity. The fact that these two approaches follow the same direction gives us some confidence regarding the ECP approach. In total, the four-electron reduction of N_2 by K_3U-N-U is exoergic by 41.2 kcal/mol, Table 2. Based on these thermodynamic considerations, we expect that K_3U-N-U can facilitate the conversion of N_2 to N_2^{4-}. Interestingly, for Cs_3-U-N-U, we obtain a reaction energy of -27.0 kcal/mol, suggesting that $N_2 \rightarrow N_2^{4-}$ conversion would also be feasible for this system.

Table 2: Calculated reaction energies, kcal/mol, for binding and four-electron reduction of N_2 by various bis-actinide siloxide complexes. The impact of thermal free energy corrections, dispersion effects and spin-orbit coupling effects are given in parenthesis.

	Priroda (PBE/L1) and Corrections			
	ΔE_{scalar}	ΔG_{scalar}	$\Delta G_{scalar-disp}$	$\Delta G_{spin-orbit}$
K_3U-N-U	-51.9	-31.7 (+20.2)	-42.2 (-10.5)	-41.2 (+1.0)
Cs_3U-N-U	-37.8	-17.4 (+20.4)	-27.5 (-10.0)	-27.0 (+0.5)
K_3Np-N-Np	-8.1	+9.2 (+17.3)	-0.5 (-9.7)	-0.7 (-0.2)
K_3Pu-N-Pu	+25.9	+42.4 (+16.5)	+34.2 (-8.3)	+32.2 (-2.0)

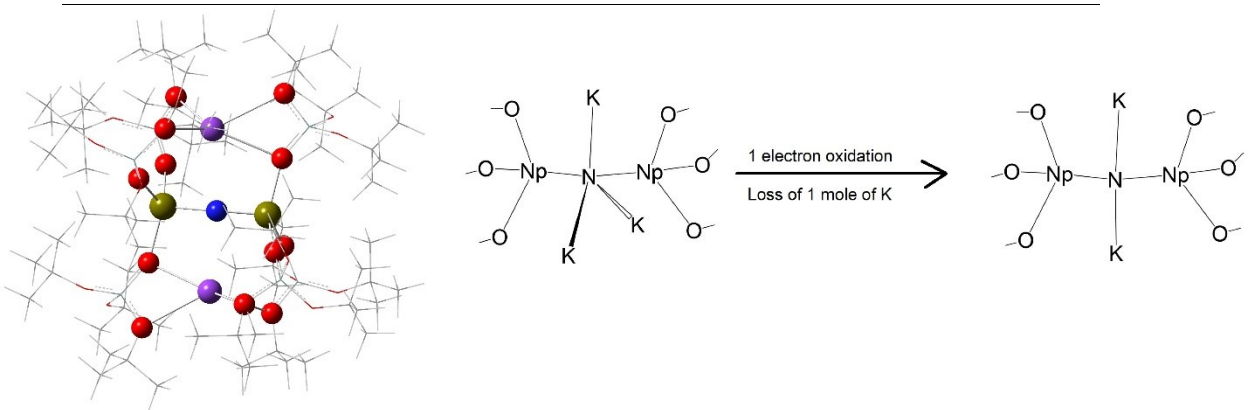

Figure 3: Structure of the K_2Np-N-Np complex with major parts of the siloxide framework represented by wireframes. Formation of this mixed oxidation state Np(III)/Np(IV) complex is shown on the right. The Np are atoms are dark orange spheres.

To understand the observed differences in the reactivities of Cs_3U-N-U and K_3U-N-U, we considered the removal of an alkali metal atom from these species to form the mixed oxidation state U(III)/U(IV) Cs_2U-N-U and K_2U-N-U analogues.[69] This is a one-electron oxidation process, Figure 3. The Np analogue of K_2U-N-U is also shown in Figure 3. Chatelain et al. have previously reported the synthesis of Cs_2U-N-U siloxide complex.[69] The reaction energies associated with the oxidation of Cs_3U-N-U and K_3U-N-U via loss of an alkali-metal atom are presented in Table 3. In addition to the thermal free energy, and long-range dispersion corrections, we also accounted for agglomeration of the expunged alkali metal atoms. The atomization energies employed for K and Cs are 21.3 and 18.2 kcal/mol, respectively.[70] We found that removal of a K atom from K_3U-N-U is endoergic by 18.5 kcal/mol while for Cs_3U-N-U, it is far easier to remove Cs, 6.9 kcal/mol, Table 3. These results suggest that Cs_3U-N-U is more amenable for opening of the siloxide framework than K_3U-N-U. The increased flexibility of the siloxide framework in Cs_3U-N-U favors formation of various possible decomposition products. The capture and reduction of N_2 no doubt requires opening of the siloxide framework. During this process, Cs_3U-N-U will more easily decompose to Cs_2U-N-U (and other species) than its K analogue. This "kinetic" explanation agrees with the experimental findings of Chatelain et al.[69] and Falcone et al.[26] As seen in Table 3, the Np and Pu analogues of K_3U-N-U are very stable against reductive decomposition via loss of potassium.

Table 3: Calculated reaction energies, kcal/mol, for removing an alkali metal (one-electron oxidation) from the Cs_3U-N-U and K_3U-N-U complexes to form mixed oxidation state U(III)/U(IV) Cs_2U-N-U and K_2U-N-U species. The reaction energies for the Np and Pu analogues of K_3U-N-U are included.

	ΔE	ΔG_{scalar}	$\Delta G_{scalar-disp}$	$\Delta G_{scalar-disp-atomization}$
K_3U-N-U	30.5	44.9 (+14.4)	39.8 (-5.1)	18.5 (-21.3)
Cs_3U-N-U	16.4	31.3 (+14.9)	25.0 (-6.3)	6.9 (-18.2)
K_3Np-N-Np	44.4	46.3 (+2.0)	50.7 (+4.4)	29.5 (-21.3)
K_3Pu-N-Pu	54.1	58.9 (+4.8)	63.2 (+4.2)	41.9 (-21.3)

3.3. Analogous Np and Pu Complexes: The calculated structural properties of K_3Np-N-Np and K_3Np-(N)(N_2)-Np as well as their Pu analogues are presented in Table 4. Comparison of K_3Np-N-Np to K_3U-N-U, Table 1, shows that the bond distances are generally within 0.02 Å of each other. This is not surprising as the ionic radius of Np(III) is only about 0.015 Å smaller than that of U(III).[71] For K_3Pu-N-Pu, the bond distances are within 0.03 Å of that of U(III), agreeing with the fact that the ionic radius of Pu(III) is only about 0.025 Å smaller than that of U(III).[71] The Mayer bond orders for these Np and Pu complexes are very similar to those of their U analogues, Table 1. However, the Np-N-Np (178.1°) and

Pu-N-Pu (177.6°) bond angles in the low-spin states of K_3Np-N-Np and K_3Pu-N-Pu, Table 4, are much larger than the U-N-U angle of K_3U-N-U, 170.5°, Table 1. We see a similar situation for the high-spin states of K_3Np-N-Np and K_3Pu-N-Pu. These larger angles are indicative of greater energy penalties for

Table 4: Average values of the calculated structural parameters of K_3Np-N-Np and K_3Np-(N)(N_2)-Np as well as their Pu analogues. The bond distances are given in Å while the bond angles are given in °.

	K_3Np-N-Np		K_3Np-(N)(N_2)-Np		K_3Pu-N-Pu		K_3Pu-(N)(N_2)-Pu	
	Singlet	Nonet	Singlet	Quintet	Singlet	Undecet	Singlet	Septet
An-N_{center}	2.110	2.113	2.100	2.097	2.115	2.103	2.126	2.103
An-$N_{dinitrogen}$			2.245	2.223			2.479	2.287
An-An	4.221	4.223	3.384	3.358	4.230	4.206	4.212	3.423
An-O	2.263	2.263	2.259	2.262	2.271	2.272	2.281	2.261
K-O	2.860	2.858	2.660-3.785	2.656-3.790	2.851	2.843	2.784-3.205	2.659-3.842
N-$N_{dinitrogen}$			1.402	1.434			1.124	1.341
An-N_{center}-An	178.1	176.1	107.4	106.4	177.6	178.9	164.5	109.0
An-$N_{dinitrogen}$-An			97.8	98.1				96.9

compressing the bis-actinide cores during N_2 capture, Scheme 1. This is also supportive of the fact that the interactions with the siloxide framework are stronger in K_3Np-N-Np and K_3Pu-N-Pu, Table 3. Examination of the frontier orbitals of the low-spin Np and Pu complexes show that their singly-occupied 5*f* orbitals (eigenvalues of -1.8 to -2.3 eV for Np and -2.1 to -2.7 eV for Pu) are all more stable than the π* orbitals of unbound N_2, Figure 4. For the Pu complex, the energy gaps between the N_2 π* orbitals and the lowest singly occupied molecular orbital (SOMO) is around 0.53 eV. We contrast this with 0.23 eV for the Np complex, Figure 4, and -0.18 eV for U, Figure 2. It thus appears that the ionization potentials of the Np and Pu 5*f* orbitals are far larger than the electron affinity of N_2, suggesting the existence of additional energy penalties against N_2 reduction by these species. Stabilization of the singly occupied 5*f* orbitals from U to Np and Pu is consistent with the increased atomic nuclear charges.

Comparison of the atomic spin densities of K_3Np-N-Np with those of K_3Np-(N)(N_2)-Np confirms that the captured N_2 moiety is reduced to N_2^{4-}. We re-iterate that this $N_2 \rightarrow N_2^{4-}$ transformation will however not occur due to the endoergicity of the whole process, Table 2. For the low-spin ground state of K_3Np-N-Np, the excess spin densities on the Np atoms are 3.89 and -3.90, confirming their $5f^4$ or Np(III) characters. After N_2 capture, the spin densities are lowered to 2.38 and -2.37, respectively, indicating that

$5f^4 \rightarrow 5f^2$ transformation of each Np is coupled to $N_2 \rightarrow N_2^{4-}$ reduction. For the analogous Pu complex, the spin densities indicate K_3Pu-N-Pu has $5f^5$ or Pu(III) centers, both in the high-spin undecet and low-spin singlet states. Interestingly, we found that the spin densities on the Pu centers remain around 5.0 ($5f^5$) after the optimization of the low-spin state of the K_3Pu-(N)(N_2)-Pu complex. Indeed, the N_2 moiety is not fully captured by the bis-actinide core in this complex, affording a structural arrangement different from those of the Np and U analogues, see Supporting Information. In contrast, for the high spin of K_3Pu-(N)(N_2)-Pu, the Pu centers have spin densities around 3.5-3.7. This suggests that N_2 is not fully reduced to N_2^{4-} by both the high-spin and low-spin states of K_3Pu-N-Pu. These findings are fully consistent with the large energy gap between the $5f$ SOMOs of K_3Pu-N-Pu and the N_2 π^* orbitals, Figure 4. The bond lengths of the captured N_2 are 1.341 and 1.124 Å in the high- and low-spin states of K_3Pu-(N)(N_2)-Pu,

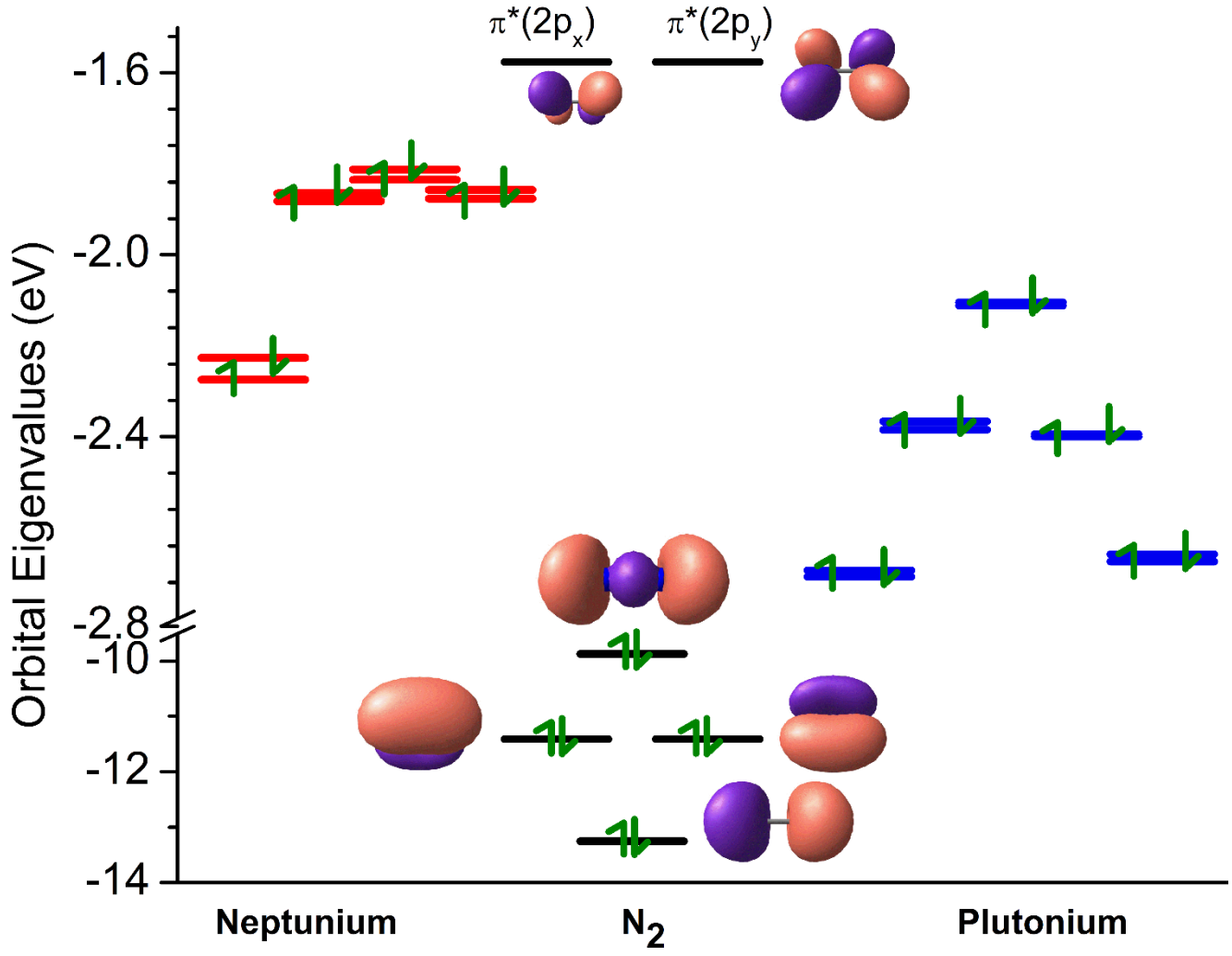

Figure 4: Comparison of the eigenvalues of the frontier orbitals of N_2 to those of the broken-symmetry singlet states of K_3Np-N-Np and K_3Pu-N-Pu. The eigenvalues were obtained at the PBE/L1 scalar-relativistic level.

respectively, Table 5. These are shorter than 1.490-1.493 Å and 1.400-1.434 Å for the analogous U and Np species, respectively, Tables 1 and 5. For comparison, the calculated bond length of unbound N_2 is 1.103 Å, in good agreement with the experimental value of 1.098 Å.[72]

The reaction energy of $N_2 \rightarrow N_2^{4-}$ conversion by the K_3Np-N-Np and K_3Pu-N-Pu complexes are shown in Table 2. In contrast to K_3U-N-U, capture and four-electron reduction of N_2 is endoergic for these species. As such, we conclude that these species cannot reduce N_2 to N_2^{4-}. Interestingly, the exoergicity of the $N_2 \rightarrow N_2^{4-}$ process follows the trend U > Np > Pu. This concurs with the trend in the N-N bond distances after N_2 capture, Tables 1 and 5, as well as the energies of the frontier orbitals of the bis-actinide nitride complexes, Figures 2 and 4.

3.4. Tuning Redox Reactivity with Ligands: The homoleptic organometallic alkyl complex, $Np[CH(SiMe_3)_2]_3$, has been suggested as a candidate for effecting small molecule activation.[37] Thus, we investigate whether modification of the ligand environments around the bis-actinide cores of K_3Np-N-Np and K_3Pu-N-Pu can alter the energetics of $N_2 \rightarrow N_2^{4-}$ conversion. To imitate the situation in $Np[CH(SiMe_3)_2]_3$, we replace the Np-O and Pu-O bonds between the actinide centers and the siloxide framework with Np-NH, Pu-NH, Np-CH_2 and Pu-CH_2 groups. The optimized structures of K_3Np-N-Np[NH] and K_3Np-(N)(N_2)-Np[NH] as well as their Np-CH_2 analogues are shown in Figure 5. The calculated structural properties of the broken-symmetry singlet states of these complexes are given in Table 5. The Np-NH and Np-CH_2 bonds of K_3Np-N-Np[NH] and K_3Np-N-Np[CH_2] are longer than the Np-O distances of K_3Np-N-Np. Similarly, the K-NH and K-CH_2 bond distances are larger than the K-O distances of K_3Np-N-Np. These trends would suggest that the framework is more amenable to opening and closing in K_3Np-N-Np[NH] and K_3Np-N-Np[CH_2]. This will make it easier to deform the bis-actinide cores of these complexes during $N_2 \rightarrow N_2^{4-}$. These are confirmed by noting that the Np-Np bond lengths are shorter for K_3Np-(N)(N_2)-Np[NH], 3.329 Å, and K_3Np-(N)(N_2)-Np[CH_2], 3.291 Å than for K_3Np-N-Np, 3.384 Å, Tables 5 and 6. Also, the N-N bonds of the captured N_2 increases from 1.402 Å to 1.451 Å and 1.472 Å as the Np-O bonds are changed to Np-NH and Np-CH_2, respectively, suggesting that it becomes gradually easier to reduce N_2. The N-N distance of 1.472 Å in K_3Np-(N)(N_2)-Np[CH_2] is already quite close to that of K_3U-(N)(N_2)-U, 1.490 Å in Table 1. We see similar trends for the Pu analogues, see Supporting Information.

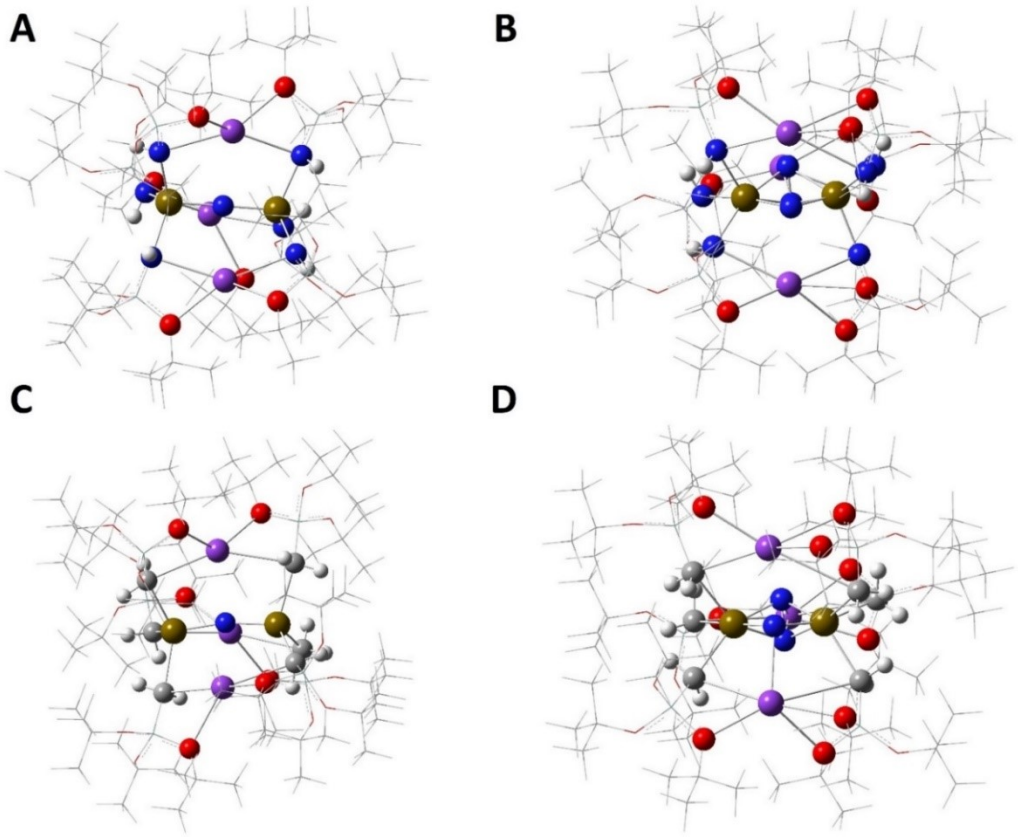

Figure 5: Structures of the K_3Np-N-Np[NH] (**A**) and K_3Np-(N)(N_2)-Np[NH] (**B**) complexes as well as their Np-CH_2 analogues, (**C**) and (**D**), respectively. The bis-actinide cores are shown with spheres, but major parts of the silyl framework are represented with wireframes for better visibility.

Table 5: Average values of the calculated structural parameters of the K_3Np-N-Np[NH] and K_3Np-(N)(N_2)-Np[NH] complexes and their [CH_2] analogues. The bond distances are given in Å while the bond angles are given in °.

	K_3Np-N-Np[NH]	K_3Np-(N)(N_2)-Np[NH]	K_3Np-N-Np[CH_2]	K_3Np-(N)(N_2)-Np[CH_2]
An-N_{center}	2.125	2.089	2.104	2.081
An-$N_{dinitrogen}$		2.220		2.194
An-An	4.249	3.329	4.170	3.291
An-NH/CH_2	2.382	2.359	2.558	2.548
K-O	2.762	2.810	2.774	2.795
K-NH/CH_2	2.953	2.988-4.013	3.116	3.171-4.096
N-$N_{dinitrogen}$		1.451		1.472
An-N_{center}-An	179.1	105.6	164.9	104.5
An-$N_{dinitrogen}$-An		97.2		97.2

The calculated reaction energies for $N_2 \rightarrow N_2^{4-}$ conversion by the Np-NH, Np-CH_2, Pu-NH and Pu-CH_2 complexes are shown in Table 6. Comparison to the results shown in Table 2 reveals that there is a trend of O < NH < CH_2 in the reaction energies. With K_3Np-N-Np[NH] and K_3Np-N-Np[CH_2], we obtained reaction energies of about -18.6 and -29.3 kcal/mol, respectively, after accounting for scalar-relativistic effects, spin-orbit coupling effects, long-range dispersion interactions and thermal free energy corrections. These values are to be compared to -0.7 kcal/mol for K_3Np-N-Np, Table 2. We conclude that K_3Np-N-Np[NH] and K_3Np-N-Np[CH_2] can effect $N_2 \rightarrow N_2^{4-}$ conversion, Table 6. These results agree

Table 6: Calculated reaction energies, kcal/mol, for binding and four-electron reduction of N_2 by bis-actinide Np and Pu complexes with modified siloxide ligand frameworks. The impact of thermal free energy corrections, dispersion effects and spin-orbit coupling effects are given in parenthesis.

	Priroda (PBE/L1) and Corrections			
	ΔE_{scalar}	ΔG_{scalar}	$\Delta G_{scalar-disp}$	$\Delta G_{spin-orbit}$
K_3Np-N-Np[NH]	-22.5	-7.8 (+14.7)	-17.4 (-9.6)	-18.6 (-1.2)
K_3Np-N-Np[CH_2]	-31.7	-20.2 (+11.5)	-25.3 (-5.1)	-29.3 (-4.0)
K_3Pu-N-Pu[NH]	+9.4		(-3.7)	
K_3Pu-N-Pu[CH_2]	-11.0		(-6.5)	(-1.1)

with the changes in the structural properties of the complexes, discussed above. For the analogous Pu complexes, the electronic reaction energy improves from +25.9 kcal/mol for K_3Pu-N-Pu, Table 2, to 9.4 kcal/mol for K_3Pu-N-Pu[NH] and -11.0 kcal/mol for K_3Pu-N-Pu[CH_2], Table 6. Unfortunately, we were only able to optimize the geometries of K_3Pu-(N)(N_2)-Pu[NH] and K_3Pu-(N)(N_2)-Pu[CH_2] with energy convergence criteria of between 1×10^{-4} and 5×10^{-5} Hartrees (0.06 – 0.03 kcal/mol). It was not possible to converge the energies of these structures with tighter criteria required for vibrational frequency analyses and estimation of the thermal free energy corrections. However, the trend towards greater exoergicity is clear from the electronic energies, Tables 2 and 6.

We confirm the abilities of K_3Np-N-Np[NH] and K_3Np-N-Np[CH_2] to capture and reduce N_2 in three ways. First, the trend towards greater exoergicity is not unique to Np and Pu. We see a similar trend for U species, Figure 6. Second, the spin-densities on the Np centers are reduced from 3.9 ($5f^4$ or Np^{3+}) to 2.1 ($5f^2$ or Np^{5+}) after N_2 transformation by these species. Third, K_3Np-N-Np[NH] and K_3Np-N-Np[CH_2] are stable against one-electron reduction via loss of a K atom, Table 7. While these species are not as stable as K_3Np-N-Np, they are much better than Cs_3U-N-U, Table 3. The SOMOs of K_3Np-N-Np[NH]

and K_3Np-N-$Np[CH_2]$ are still below the π^* orbitals of N_2, Figure 6. It thus appears that these species sacrifice some framework stability in order to be able to push electrons from the Np centers into N_2-based orbitals. Based on the data in Tables 6 and 7 as well as Figure 6, K_3Np-N-Np[NH] is the most promising candidate for effecting $N_2 \rightarrow N_2^{4-}$ conversion by a trans-uranium complex.

Table 7: Calculated reaction energies, kcal/mol, for removing an alkali metal (one-electron oxidation) from K_3Np-N-Np[NH] and K_3Np-N-$Np[CH_2]$ as well as their Pu analogues.

	ΔE	ΔG_{scalar}	$\Delta G_{scalar-disp}$	$\Delta G_{scalar-disp-atomization}$
K_3Np-N-Np[NH]	38.7	43.4 (+4.6)	43.3 (-0.1)	22.0 (-21.3)
K_3Np-N-$Np[CH_2]$	36.4	34.5 (-1.9)	32.6 (-1.9)	11.3 (-18.2)
K_3Pu-N-Pu[NH]	52.0			
K_3Pu-N-$Pu[CH_2]$	44.1			

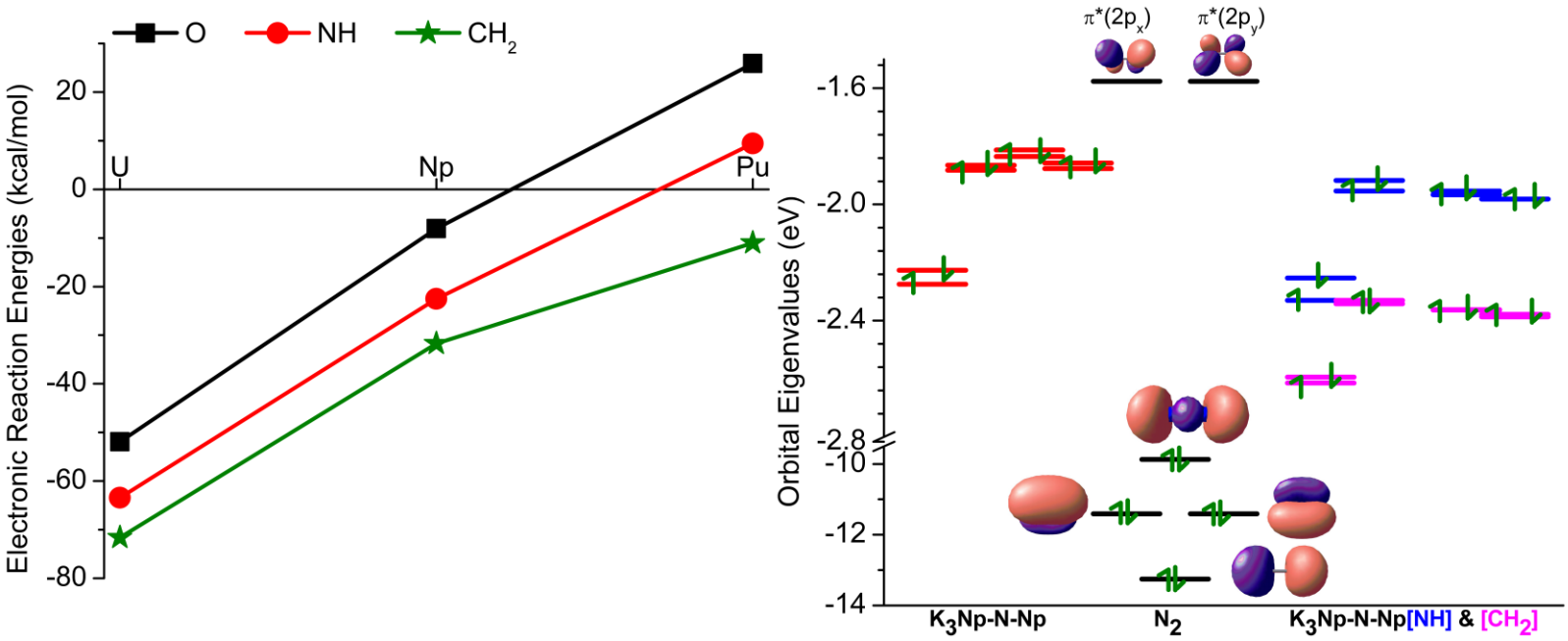

Figure 6: (***left***) Trend in the $N_2 \rightarrow N_2^{4-}$ electronic reaction energies for bis-actinide complexes. (***right***) Comparison of the eigenvalues of the frontier orbitals of N_2 to those of the broken-symmetry singlet states of K_3Np-N-Np (red), K_3Np-N-Np[NH] (blue) and K_3Np-N-$Np[CH_2]$ (pink).

4. CONCLUSIONS

To explore the possibility of small molecule activation by trans-uranium organometallic actinide complexes, we have examined the structural, electronic and reactivity properties of a bis-uranium nitride (U-N-U) complex that is able to facilitate the capture, reduction and functionalization of nitrogen. This

complex was recently synthesized and characterized. We compared the properties the properties of this uranium complex to those of its neptunium and plutonium analogues by means of approximate scalar-relativistic and spin-orbit coupled DFT calculations. This level of theory is sufficient to allow for a good determination of the trends in the properties of these complexes. After modeling the equilibrium structures of the bis-actinide nitride complexes, we calculated the reaction energies for the capture and four-electron reduction of nitrogen ($N_2 \rightarrow N_2^{4-}$) using reaction schema that accounts for thermal free energy corrections as well as long-range dispersion interactions. The influence of the ligand environment on the reduction of nitrogen by these species was examined in two ways. First, we probed the role of the alkali-metal ions that serve to hold the siloxide framework encasing the bis-actinide cores. Specifically, we compared the U-N-U reactivity within a potassium (K_3U-N-U) or cesium (Cs_3U-N-U) siloxide framework. Second, we examined the possibility of altering the redox reactivities of the Np and Pu complexes by changing the ligand frameworks from Np-O and Pu-O to Np-NH, Np-CH_2, Pu-NH and Pu-CH_2 species.

We find that K_3U-N-U can capture and reduce N_2. This is based on analysis of the reaction energy for the $N_2 \rightarrow N_2^{4-}$ process as well as the bond orders and spin densities. Based on these thermodynamic, electronic and structural properties, we found that Cs_3U-N-U can also effect this transformation. However, the latter is more susceptible to decomposition via a one-electron oxidation process involving loss of an alkali atom. This process is associated with opening of the siloxide framework and will occur during N_2 capture. Based on this "kinetic" factor, we conclude that N_2 capture and reduction by Cs_3U-N-U will yield complex chemistry unlike the situation for K_3U-N-U where $N_2 \rightarrow N_2^{4-}$ is the favored transformation. These conclusions agree with previous experimental observations.

Using similar considerations, we conclude that the Np and Pu analogues of K_3U-N-U cannot capture and reduce N_2 to N_2^{4-}. The $N_2 \rightarrow N_2^{4-}$ process is significantly more endoergic for the trans-uranium complexes. Detailed analyses of the differences between the U, Np and Pu systems allowed us to propose that systems with An-NH and An-CH_2 (where An represent actinide atoms) metal-ligand interactions are possible opportunities for effecting this small-molecule activation by the Np and Pu complexes. Based on similar analyses as described earlier, we find that K_3Np-N-Np[NH] (the oxo atoms of the siloxide framework are replaced by NH groups) and possibly K_3Np-N-Np[CH_2], can reduce N_2 to N_2^{4-}. This is possible through a delicate balance between the stability of the ligand framework and the ionization potentials of the actinide complex. These findings highlight a way forward for achieving small-molecule activation with trans-uranium complexes.

ASSOCIATED CONTENT

Supporting Information.

The SI contains the geometries of all the molecules considered in this work. This material is available free of charge via the Internet at http://pubs.acs.org.

AUTHOR INFORMATION

Corresponding Authors

*S.O.O.: E-mail: sodoh@unr.edu

Notes

¶ These authors contributed equally to this work. We declare no competing financial interest.

ACKNOWLEDGMENT

This material is based upon work supported by the National Science Foundation under Grant No. 1800387.

REFERENCES

(1) Fryzuk, M. D.; Johnson, S. A. The continuing story of dinitrogen activation. *Coordin. Chem. Rev.* **2000**, *200*, 379.

(2) Shaver, M. P.; Fryzuk, M. D. Activation of molecular nitrogen: Coordination, cleavage and functionalization of N_2 mediated by metal complexes. *Adv. Synth. Catal.* **2003**, *345*, 1061.

(3) Crossland, J. L.; Tyler, D. R. Iron-dinitrogen coordination chemistry: Dinitrogen activation and reactivity. *Coordin. Chem. Rev.* **2010**, *254*, 1883.

(4) Fryzuk, M. D. Activation and functionalization of molecular nitrogen by metal complexes. *Chem. Rec.* **2003**, *3*, 2.

(5) Hazari, N. Homogeneous iron complexes for the conversion of dinitrogen into ammonia and hydrazine. *Chem. Soc. Rev.* **2010**, *39*, 4044.

(6) Hidai, M.; Mizobe, Y. Recent advances in the chemistry of dinitrogen complexes. *Chem. Rev.* **1995**, *95*, 1115.

(7) MacLeod, K. C.; Holland, P. L. Recent developments in the homogeneous reduction of dinitrogen by molybdenum and iron. *Nat. Chem.* **2013**, *5*, 559.

(8) Nishibayashi, Y. Recent progress in transition-metal-catalyzed reduction of molecular dinitrogen under ambient reaction conditions. *Inorg. Chem.* **2015**, *54*, 9234.

(9) Liu, H. *Ammonia Synthesis Catalysts*; World Scientific Publishing Company, 2013.

(10) Smith, B. E. Nitrogenase reveals its inner secrets. *Science* **2002**, *297*, 1654.

(11) Hidai, M. Chemical nitrogen fixation by molybdenum and tungsten complexes. *Coordin. Chem. Rev.* **1999**, *185-6*, 99.

(12) Murakami, J.; Yamaguchi, W. Reduction of N_2 by supported tungsten clusters gives a model of the process by nitrogenase. *Sci. Rep-UK* **2012**, *2*, 407.

(13) Schrock, R. R. Catalytic reduction of dinitrogen to ammonia at a single molybdenum center. *Accounts Chem. Res.* **2005**, *38*, 955.

(14) Shilov, A.; Denisov, N.; Efimov, O.; Shuvalov, N.; Shuvalov.N; Shilova, A. New nitrogenase model for reduction of molecular nitrogen in protonic media. *Nature* **1971**, *231*, 460.

(15) Wickramasinghe, L. A.; Ogawa, T.; Schrock, R. R.; Muller, P. Reduction of dinitrogen to ammonia catalyzed by molybdenum diamido complexes. *J. Am. Chem. Soc.* **2017**, *139*, 9132.

(16) Yandulov, D. V.; Schrock, R. R. Catalytic reduction of dinitrogen to ammonia at a single molybdenum center. *Science* **2003**, *301*, 76.

(17) Berthet, J. C.; Thuery, P.; Ephritikhine, M. Polyimido clusters of neodymium and uranium, including a cluster with an $M_6(\mu_3\text{-}N)_8$ core. *Eur. J. Inorg. Chem.* **2008**, 5455.

(18) Campazzi, E.; Solari, E.; Floriani, C.; Scopelliti, R. The fixation and reduction of dinitrogen using lanthanides: praseodymium and neodymium meso-octaethylporphyrinogen-dinitrogen complexes. *Chem. Commun.* **1998**, 2603.

(19) Chatt, J.; Dilworth, J. R.; Richards, R. L. Recent advances in chemistry of nitrogen fixation. *Chem. Rev.* **1978**, *78*, 589.

(20) Evans, W. J.; Allen, N. T.; Ziller, J. W. Expanding divalent organolanthanide chemistry: The first organothulium(II) complex and the in situ organodysprosium(II) reduction of dinitrogen. *Angew. Chem. Int. Edit.* **2001**, *41*, 359.

(21) Evans, W. J.; Fang, M.; Zucchi, G.; Furche, F.; Ziller, J. W.; Hoekstra, R. M.; Zink, J. I. Isolation of dysprosium and yttrium complexes of a three-electron reduction product in the activation of dinitrogen, the $(N_2)^{3-}$ radical. *J. Am. Chem. Soc.* **2009**, *131*, 11195.

(22) Evans, W. J.; Lee, D. S.; Rego, D. B.; Perotti, J. M.; Kozimor, S. A.; Moore, E. K.; Ziller, J. W. Expanding dinitrogen reduction chemistry to trivalent lanthanides via the LnZ_3/alkali metal reduction system: Evaluation of the generality of forming $Ln_2(\mu\text{-}\eta^2\text{:}\eta^2\text{-}N_2)$ complexes via LnZ_3/K. *J. Am. Chem. Soc.* **2004**, *126*, 14574.

(23) Evans, W. J.; Lorenz, S. E.; Ziller, J. W. Investigating metal size effects in the $Ln_2(\mu\text{-}\eta^2\text{:}\eta^2\text{-}N_2)$ reduction system: Reductive reactivity with complexes of the largest and smallest trivalent lanthanide ions, La^{3+} and Lu^{3+}. *Inorg. Chem.* **2009**, *48*, 2001.

(24) Evans, W. J.; Zucchi, G.; Ziller, J. W. Dinitrogen reduction by Tm(II), Dy(II), and Nd(II) with simple amide and aryloxide ligands. *J. Am. Chem. Soc.* **2003**, *125*, 10.

(25) Gardiner, M. G.; Stringer, D. N. Dinitrogen and related chemistry of the lanthanides: A review of the reductive capture of dinitrogen, as well as mono- and di-aza containing ligand dhemistry of relevance to known and postulated metal mediated dinitrogen derivatives. *Materials* **2010**, *3*, 841.

(26) Falcone, M.; Chatelain, L.; Scopelliti, R.; Zivkovic, I.; Mazzanti, M. Nitrogen reduction and functionalization by a multimetallic uranium nitride complex. *Nature* **2017**, *547*, 332.

(27) Liu, H. *Ammonia synthesis catalysts*.

(28) Arnold, P. L. Uranium-mediated activation of small molecules. *Chem. Commun.* **2011**, *47*, 9005.

(29) Arnold, P. L.; Turner, Z. R. Carbon oxygenate transformations by actinide compounds and catalysts. *Nat. Rev. Chem.* **2017**, *1*, 0002.

(30) Arnold, P. L.; Turner, Z. R.; Germeroth, A. I.; Casely, I. J.; Nichol, G. S.; Bellabarba, R.; Tooze, R. P. Carbon monoxide and carbon dioxide insertion chemistry of f-block N-heterocyclic carbene complexes. *Dalton T.* **2013**, *42*, 1333.

(31) Castro-Rodriguez, I.; Meyer, K. Small molecule activation at uranium coordination complexes: control of reactivity via molecular architecture. *Chem. Commun.* **2006**, 1353.

(32) Falcone, M.; Chatelain, L.; Scopelliti, R.; Mazzanti, M. CO cleavage and CO_2 functionalization under mild conditions by a multimetallic CsU_2 nitride complex. *Chimia* **2017**, *71*, 209.

(33) Falcone, M.; Kefalidis, C. E.; Scopelliti, R.; Maron, L.; Mazzanti, M. Facile CO cleavage by a multimetallic CsU_2 nitride complex. *Angew. Chem. Int. Edit.* **2016**, *55*, 12290.

(34) Falcone, M.; Poon, L. N.; Tirani, F. F.; Mazzanti, M. Reversible dihydrogen activation and hydride transfer by a uranium nitride complex. *Angew. Chem. Int. Edit.* **2018**, *57*, 3697.

(35) Summerscales, O. T.; Cloke, F. G. N. In *Organometallic and Coordination Chemistry of the Actinides*; AlbrechtSchmitt, T. E., Ed. 2008; Vol. 127, p 87.

(36) Zhang, L.; Zhang, C. C.; Hou, G. H.; Zi, G. F.; Walter, M. D. Small-molecule activation mediated by a uranium bipyridyl metallocene. *Organometallics* **2017**, *36*, 1179.

(37) Arnold, P. L.; Dutkiewicz, M. S.; Walter, O. Organometallic neptunium chemistry. *Chem. Rev.* **2017**, *117*, 11460.

(38) Laikov, D. N. A new class of atomic basis functions for accurate electronic structure calculations of molecules. *Chem. Phys. Lett.* **2005**, *416*, 116.

(39) Laikov, D. N. Neglect of four- and approximation of one-, two-, and three-center two-electron integrals in a symmetrically orthogonalized basis. *J. Comput. Chem.* **2007**, *28*, 698.

(40) Laikov, D. N.; Ustynyuk, Y. A. PRIRODA-04: a quantum-chemical program suite. New possibilities in the study of molecular systems with the application of parallel computing. *Russ. Chem. B+* **2005**, *54*, 820.

(41) Perdew, J. P.; Burke, K.; Ernzerhof, M. Generalized gradient approximation made simple. *Phys. Rev. Lett.* **1996**, *77*, 3865.

(42) Gritsenko, O. V.; Schipper, P. R. T.; Baerends, E. J. Exchange and correlation energy in density functional theory: Comparison of accurate density functional theory quantities with traditional Hartree-Fock based ones and generalized gradient approximations for the molecules Li_2, N_2, F_2. *J. Chem. Phys.* **1997**, *107*, 5007.

(43) Dyall, K. G. An exact separation of the spin-free and spin-dependent terms of the Dirac-Coulumb-Breit Hamiltonian. *J. Chem. Phys.* **1994**, *100*, 2118.

(44) Mayer, I. Bond order and valence indices: A personal account. *J. Comput. Chem.* **2007**, *28*, 204.

(45) Mulliken, R. S. Electronic population analysis on LCAO–MO molecular wave functions. I. *J. Chem. Phys.* **1955**, *23*, 1833.

(46) Hirshfeld, F. L. Bonded-atom fragments for describing molecular charge densities. *Theor. Chim. Acta* **1977**, *44*,

(47) Grimme, S.; Antony, J.; Ehrlich, S.; Krieg, H. A consistent and accurate ab initio parametrization of density functional dispersion correction (DFT-D) for the 94 elements H-Pu. *J. Chem. Phys.* **2010**, *132*, 154104.

(48) Grimme, S.; Ehrlich, S.; Goerigk, L. Effect of the damping function in dispersion corrected density functional theory. *J. Comput. Chem.* **2011**, *32*, 1456.

(49) Johnson, E. R.; Becke, A. D. A post-Hartree-Fock model of intermolecular interactions: Inclusion of higher-order corrections. *J. Chem. Phys.* **2006**, *124*, 174104.

(50) Frisch, M. J.; Trucks, G. W.; Schlegel, H. B.; Scuseria, G. E.; Robb, M. A.; Cheeseman, J. R.; Scalmani, G.; Barone, V.; Petersson, G. A.; Nakatsuji, H.; Li, X.; Caricato, M.; Marenich, A. V.; Bloino, J.; Janesko, B. G.; Gomperts, R.; Mennucci, B.; Hratchian, H. P.; Ortiz, J. V.; Izmaylov, A. F.; Sonnenberg, J. L.; Williams; Ding, F.; Lipparini, F.; Egidi, F.; Goings, J.; Peng, B.; Petrone, A.; Henderson, T.; Ranasinghe, D.; Zakrzewski, V. G.; Gao, J.; Rega, N.; Zheng, G.; Liang, W.; Hada, M.; Ehara, M.; Toyota, K.; Fukuda, R.; Hasegawa, J.; Ishida, M.; Nakajima, T.; Honda, Y.; Kitao, O.; Nakai, H.; Vreven, T.; Throssell, K.; Montgomery Jr., J. A.; Peralta, J. E.; Ogliaro, F.; Bearpark, M. J.; Heyd, J. J.; Brothers, E. N.; Kudin, K. N.; Staroverov, V. N.; Keith, T. A.; Kobayashi, R.; Normand, J.; Raghavachari, K.; Rendell, A. P.; Burant, J. C.; Iyengar, S. S.; Tomasi, J.; Cossi, M.; Millam, J. M.; Klene, M.; Adamo, C.; Cammi, R.; Ochterski, J. W.; Martin, R. L.; Morokuma, K.; Farkas, O.; Foresman, J. B.; Fox, D. J. *Gaussian 16 Rev. B.01*, Gaussian Inc. Wallingford CT, 2016.

(51) Becke, A. D. Density-functional thermochemistry .3. The role of exact exchange. *J. Chem. Phys.* **1993**, *98*, 5648.

(52) Lee, C. T.; Yang, W. T.; Parr, R. G. Development of the Colle-Salvetti correlation-energy formula into a functional of the electron-density. *Phys. Rev. B* **1988**, *37*, 785.

(53) Weigend, F.; Ahlrichs, R. Balanced basis sets of split valence, triple zeta valence and quadruple zeta valence quality for H to Rn: Design and assessment of accuracy. *Phys. Chem. Chem. Phys.* **2005**, *7*, 3297.

(54) Valiev, M.; Bylaska, E. J.; Govind, N.; Kowalski, K.; Straatsma, T. P.; Van Dam, H. J. J.; Wang, D.; Nieplocha, J.; Apra, E.; Windus, T. L.; de Jong, W. NWChem: A comprehensive and scalable open-source solution for large scale molecular simulations. *Comput. Phys. Commun.* **2010**, *181*, 1477.

(55) Ermler, W. C.; Ross, R. B.; Christiansen, P. A. Ab initio relativistic effective potentials with spin-orbit operators. VI. Fr through Pu. *Int. J. Quantum Chem.* **1991**, *40*, 829.

(56) Hurley, M. M.; Pacios, L. F.; Christiansen, P. A.; Ross, R. B.; Ermler, W. C. Ab initio relativistic effective potentials with spin-orbit operators .II. K through Kr. *J. Chem. Phys.* **1986**, *84*, 6840.

(57) Pacios, L. F.; Christiansen, P. A. Ab initio relativistic effective potentials with spin-orbit operators .I. Li through Ar. *J. Chem. Phys.* **1985**, *82*, 2664.

(58) Ross, R. B.; Powers, J. M.; Atashroo, T.; Ermler, W. C.; Lajohn, L. A.; Christiansen, P. A. Ab initio relativistic effective potentials with spin-orbit operators .IV. Cs through Rn. *J. Chem. Phys.* **1990**, *93*, 6654.

(59) Zhang, Z. Y. Spin-orbit DFT with analytic gradients and applications to heavy element compounds. *Theor. Chem. Acc.* **2014**, *133*, 1588.

(60) Jiao, Y. G.; Dibble, T. S. Quality structures, vibrational frequencies, and thermochemistry of the products of reaction of BrHg center dot with NO_2, HO_2, ClO, BrO, and IO. *J. Phys. Chem. A* **2015**, *119*, 10502.

(61) Kim, J.; Ihee, H.; Lee, Y. S. Spin-orbit density functional and ab initio study of HgXn (X=F, Cl, Br, and I; n=1, 2, and 4). *J. Chem. Phys.* **2010**, *133*, 144309.

(62) Baerends, E. J.; Ziegler, T.; Atkins, A. J.; Autschbach, J.; Bashford, D.; Baseggio, O.; Bérces, A.; Bickelhaupt, F. M.; Bo, C.; Boerritger, P. M.; Cavallo, L.; Daul, C.; Chong, D. P.; Chulhai, D. V.; Deng, L.; Dickson, R. M.; Dieterich, J. M.; Ellis, D. E.; van Faassen, M.; Ghysels, A.; Giammona, A.; van Gisbergen, S. J. A.; Goez, A.; Götz, A. W.; Gusarov, S.; Harris, F. E.; van den Hoek, P.; Hu, Z.; Jacob, C. R.; Jacobsen, H.; Jensen, L.; Joubert, L.; Kaminski, J. W.; van Kessel, G.; König, C.; Kootstra, F.; Kovalenko, A.; Krykunov, M.; van Lenthe, E.; McCormack, D. A.; Michalak, A.; Mitoraj, M.; Morton, S. M.; Neugebauer, J.; Nicu, V. P.; Noodleman, L.; Osinga, V. P.; Patchkovskii, S.; Pavanello, M.; Peeples, C. A.; Philipsen, P. H. T.; Post, D.; Pye, C. C.; Ramanantoanina, H.; Ramos, P.; Ravenek, W.; Rodríguez, J. I.; Ros, P.; Rüger, R.; Schipper, P. R. T.; Schlüns, D.; van Schoot, H.; Schreckenbach, G.; Seldenthuis, J. S.; Seth, M.; Snijders, J. G.; Sol\`a, M.; M., S.; Swart, M.; Swerhone, D.; te Velde, G.; Tognetti, V.; Vernooijs, P.; Versluis, L.; Visscher, L.; Visser, O.; Wang, F.; Wesolowski, T. A.; van Wezenbeek, E. M.; Wiesenekker, G.; Wolff, S. K.; Woo, T. K.; Yakovlev, A. L. *ADF2017, SCM, Theoretical Chemistry, Vrije Universiteit, Amsterdam, The Netherlands,* https://www.scm.com.

(63) Guerra, C. F.; Snijders, J. G.; te Velde, G.; Baerends, E. J. Towards an order-N DFT method. *Theor. Chem. Acc.* **1998**, *99*, 391.

(64) te Velde, G.; Bickelhaupt, F. M.; Baerends, E. J.; Guerra, C. F.; Van Gisbergen, S. J. A.; Snijders, J. G.; Ziegler, T. Chemistry with ADF. *J. Comput. Chem.* **2001**, *22*, 931.

(65) Van Lenthe, E.; Snijders, J. G.; Baerends, E. J. The zero-order regular approximation for relativistic effects: The effect of spin-orbit coupling in closed shell molecules. *J. Chem. Phys.* **1996**, *105*, 6505.

(66) Chong, D. P. Augmenting basis set for time-dependent density functional theory calculation of excitation energies: Slater-type orbitals for hydrogen to krypton. *Mol. Phys.* **2005**, *103*, 749.

(67) Chong, D. P.; Van Lenthe, E.; Van Gisbergen, S.; Baerends, E. J. Even-tempered slater-type orbitals revisited: From hydrogen to krypton. *J. Comput. Chem.* **2004**, *25*, 1030.

(68) Van Lenthe, E.; Baerends, E. J. Optimized slater-type basis sets for the elements 1-118. *J. Comput. Chem.* **2003**, *24*, 1142.

(69) Chatelain, L.; Scopelliti, R.; Mazzanti, M. Synthesis and structure of nitride-bridged uranium(III) complexes. *J. Am. Chem. Soc.* **2016**, *138*, 1784.

(70) Cox, J. D.; Wagman, D. D.; Medvedev, V. A. *CODATA key values for thermodynamics*; Hemisphere Publishing Corp.: New York, 1989.

(71) Shannon, R. D. Revised effective ionic-radii and systematic studies of interatomic distances in halides and chalcogenides *Acta Crystallogr. A* **1976**, *32*, 751.

(72) Huber, K. P.; Herzberg, G. *Constants of diatomic molecules*; Prentice-Hall: New York, 1979; Vol. IV.

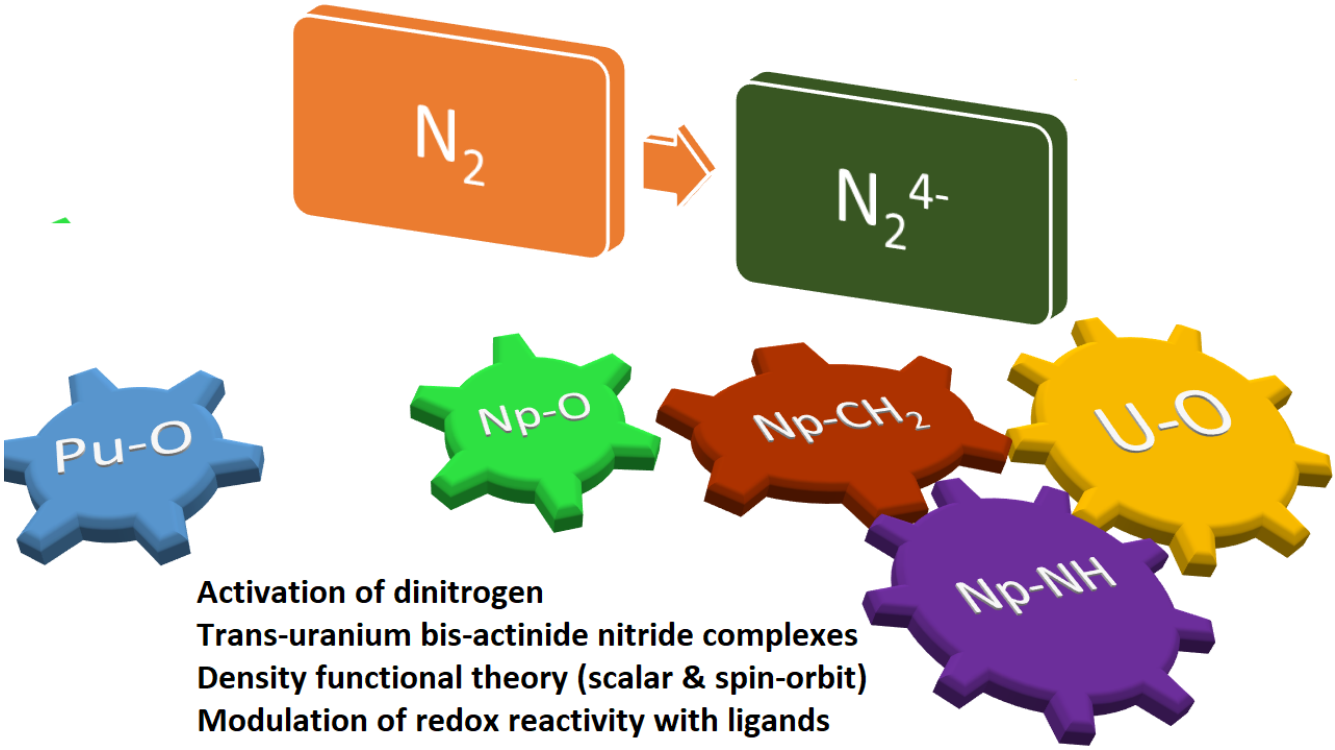

Synopsis: Modification of the ligand environment around the actinide centers allowed for the four-electron activation of dinitrogen by trans-uranium complexes. Small-molecule activation by neptunium and plutonium complexes are very rare, in contrast to their uranium analogues. Scalar-relativistic and spin-orbit corrected density functional theory show that the redox reactivities of the trans-uranium complexes can be modulated with ligands to an extent that they start resembling their uranium analogue.